The Role of Cold Pools in Tropical Oceanic Convective Systems

LEAH D. GRANT

Department of Atmospheric Science, Colorado State University, Fort Collins, Colorado

TODD P. LANE

School of Earth Sciences, and Australian Research Council Centre of Excellence for Climate Extremes, University of Melbourne, Melbourne, Victoria, Australia

SUSAN C. VAN DEN HEEVER

Department of Atmospheric Science, Colorado State University, Fort Collins, Colorado

(Manuscript received 21 November 2017, in final form 18 April 2018)

ABSTRACT

The processes governing organized tropical convective systems are not completely understood despite their important influences on the tropical atmosphere and global circulation. In particular, cold pools are known to influence the structure and maintenance of midlatitude systems via Rotunno–Klemp–Weisman (RKW) theory, but cold pools may interact differently with tropical convection because of differences in cold pool strength and environmental shear. In this study, the role of cold pools in organized oceanic tropical convective systems is investigated, including their influence on system intensity, mesoscale structure, and propagation. To accomplish this goal, high-resolution idealized simulations are performed for two different systems that are embedded within a weakly sheared cloud population approaching radiative–convective equilibrium. The cold pools are altered by changing evaporation rates below cloud base in a series of sensitivity tests. The simulations demonstrate surprising findings: when cold pools are weakened, the convective systems become more intense. However, their propagation speeds and mesoscale structure are largely unaffected by the cold pool changes. Passive tracers introduced into the cold pools indicate that the convection intensifies when cold pools are weakened because cold pool air is entrained into updrafts, thereby reducing updraft intensity via the cold pools' initial negative buoyancy. Gravity waves, rather than cold pools, appear to be the important modulators of system propagation and mesoscale structure. These results reconfirm that RKW theory does not fully explain the behavior of tropical oceanic convective systems, even those that otherwise appear consistent with RKW thinking.

1. Introduction

Despite the importance of organized tropical convective systems to the global circulation (Riehl and Malkus 1958) and to the state of the tropical atmosphere including the tropical rainfall budget (Nesbitt et al. 2000, 2006; Tan et al. 2013), the dynamics of linearly organized midlatitude convective systems are arguably better understood than those of tropical systems. Numerous papers on midlatitude convection have highlighted the important role of cold pools in linearly organized systems via Rotunno–Klemp–Weisman (RKW) theory (Rotunno et al. 1988; Weisman and Rotunno 2004). This theory postulates that the circulation on the downshear side of the cold pool, which behaves as a density current, and the wind shear in the inflow environment interact to influence the convective system structure (e.g., its tilt) and intensity and control its maintenance. Rotunno et al. (1988, p. 463) state, "We argue that these results describe the physics of both midlatitude and tropical squall lines."

Observational studies of linearly organized tropical convective systems have documented wide variability in the strength of the low- and midlevel environmental shear, convective-line orientation relative to the shear vector, thermodynamic characteristics of the environment, and system propagation speeds (e.g., Houze and Cheng 1977; Zipser 1977; LeMone et al. 1998; Johnson et al. 2005). Other studies of tropical convective systems

Corresponding author: Leah D. Grant, leah.grant@colostate.edu

DOI: 10.1175/JAS-D-17-0352.1

have often utilized idealized numerical simulations, typically over an ocean surface. Some studies have focused on feedbacks between radiative heating, surface fluxes, and cloud cover (e.g., Held et al. 1993; Bretherton et al. 2005; Stephens et al. 2008) and the importance of cold pools (Tompkins 2001; Jeevanjee and Romps 2013; Muller and Bony 2015) in organizing convection, while still others have demonstrated the influence of gravity waves on convective initiation and clustering (e.g., Clark et al. 1986; Mapes 1993; Lac et al. 2002; Fovell 2002; Tulich and Mapes 2008; Lane and Zhang 2011). Slow-moving, shear-parallel tropical squall lines have rarely been simulated, however. Several authors who have evaluated shear-perpendicular tropical squall lines found consistent behavior with RKW theory (Nicholls et al. 1988; Keenan and Carbone 1992; Robe and Emanuel 2001), though others have not (Moncrieff and Miller 1976; Webster et al. 2002; Tulich and Kiladis 2012). More recently, Lane and Moncrieff (2015, hereafter LM15) and Moncrieff and Lane (2015, hereafter ML15) investigated the morphology of two types of convective systems in sheared tropical oceanic environments whose behavior did not conform to that expected from RKW theory. LM15 investigated an ''upshear-propagating regime.'' In those systems, it appeared that the cold pool defined the system's propagation speed but that the cold pool was coupled to a ducted gravity wave, such that the region of preferred convective initiation was on the upshear side of the cold pool. In ML15, the vertical wind shear was marginally weaker than in LM15, and the convective systems propagated downshear. The weak cold pools in this ''downshear-propagating regime'' did not appear to control the propagation of the convective systems.

As the above discussion suggests, it is unclear exactly how important cold pools are to the organization of tropical convection and to tropical convective system behavior in different environments. The goal of our study is therefore to investigate the role of cold pools in tropical convective systems. We address the following question: How do cold pools influence tropical convective system evolution and characteristics such as intensity, mesoscale structure, and propagation mechanisms? Based on our prior knowledge of cold pools and their demonstrated importance for convective initiation (e.g., Tompkins 2001) and convective system maintenance (e.g., LM15) in the tropics, we hypothesized that if we were to weaken or remove the cold pools, the convective systems would be weaker, would propagate more slowly, or would fail to maintain their organization. We tested our hypothesis using idealized simulations (described in section 2), and as demonstrated in section 3, we were wrong on all accounts. Instead, we show that the weakening of the cold pools acts to intensify the organized systems (section 3a) and has little influence on the systems' propagation, longevity, and structure (section 3b); we then explore physical explanations for these results (sections 3c and 3d).

2. Description of simulations

a. *RCE-BASE simulation*

To address our hypothesis and investigate the role of cold pools in tropical convective systems, we ran idealized simulations using the Regional Atmospheric Modeling System (RAMS), version 6.1.18 (Cotton et al. 2003; Saleeby and van den Heever 2013). RAMS has been successfully used to investigate tropical convection in a number of prior studies (e.g., Stephens et al. 2004, 2008; Posselt et al. 2008; Storer and van den Heever 2013) and is therefore a useful tool for this work. We used the radiative–convective equilibrium (RCE) framework, which is an idealized approximation to the state of the tropical maritime atmosphere (Manabe and Strickler 1964; Tompkins and Craig 1998). Linearly oriented convective systems, which are commonly observed over tropical oceans (Houze and Cheng 1977; LeMone et al. 1998; Johnson et al. 2005; Liu and Zipser 2013), emerge spontaneously in large-domain channel RCE simulations (e.g., Held et al. 1993; Grabowski and Moncrieff 2001). Our approach was to examine two different convective systems embedded within the initial simulation's domain (RCE-BASE); these systems occurred about 20 days into the simulation when the environment in RCE-BASE was approaching its equilibrium state.

The RCE-BASE simulation domain was a long channel with dimensions 3000 km × 200 km × 25 km, 1-km horizontal grid spacing, and 75 stretched vertical levels with vertical grid spacing that varied from 70 m near the surface to 500 m aloft. The main time step was 5 s. Lateral boundary conditions were periodic, a Rayleigh damping layer was included in the topmost 4 km, and the lower boundary was an ocean surface with 300-K sea surface temperature. Surface–atmosphere energy and momentum exchanges were calculated using bulk formulas following Louis (1979) with the minimum wind speed increased to $7\,\mathrm{m\,s^{-1}}$ (only for the purpose of the flux calculations) so that the domain-averaged surface latent and sensible heat fluxes were comparable to observed tropical oceanic values of order 100 and $10\,\mathrm{W\,m^{-2}}$, respectively. Such wind thresholds applied to flux calculations are typical in many models. Without this adjustment, surface fluxes are unrealistically low given the low wind speeds (see below). Other physical parameterizations used in RAMS include the Harrington (1997) two-stream radiation scheme updated every 5 min of simulation time; an anisotropic Smagorinsky (1963) turbulence scheme with stability modifications by Hill (1974) and diffusion coefficients calculated for perturbation fields; and a two-moment bulk

microphysics scheme with three liquid (cloud, drizzle, rain) and five ice (pristine ice, snow, aggregates, graupel, hail) categories and bin-emulating procedures for droplet nucleation, riming, and sedimentation (Meyers et al. 1997; Saleeby and Cotton 2004, 2008). The shape parameter in the gamma distribution was set to 4 for cloud and drizzle and 2 for all other species, which are typical values for these hydrometeor categories. The horizontally homogeneous but vertically varying initial aerosol profile was exponentially decreasing with a surface concentration of 100 mg^{-1} and a scale height of 7 km. Aerosols were given a solubility of 90% for droplet nucleation and could nucleate ice following DeMott et al. (2010). Sources and sinks of aerosol number were not included, and aerosols were not radiatively active.

The 0000 UTC 5 December 1992 TOGA COARE sounding was used as the initial thermodynamic profile but with zero wind throughout the atmosphere, as in Stephens et al. (2004). Random temperature perturbations of maximum amplitude 0.1 K were introduced over the lowest 500 m AGL to initialize boundary layer inhomogeneity. Following prior RCE studies, the diurnal cycle was excluded by employing a constant solar zenith angle of 50° and the solar constant was changed to 695.41 $W m^{-2}$, which resulted in a top-of-atmosphere insolation of 447 $W m^{-2}$, the tropical atmosphere annual mean (Posselt et al. 2012). Deep convection developed after several days because of atmospheric destabilization by radiative cooling and surface fluxes. The mean winds evolve throughout the simulation, and cross-longitudinal circulations develop such that shear of the horizontal winds arises as time progresses. This evolution allows the convective systems and the environmental flow to work in concert; that is, convective momentum fluxes interact consistently with the wind profile to modify the shear (e.g., Lane and Moncrieff 2010).

By day 20, there are multiple moist and dry bands within the channel domain, a common characteristic of channel RCE simulations (e.g., Stephens et al. 2008). Envelopes of organized convection pulse within each moist band (Fig. 1). We selected and simulated two convective systems from RCE-BASE at higher resolution (section 2b) starting at day 20, following a one-way nesting approach similar to McGee and van den Heever (2014). At day 20, the simulation has not yet reached an equilibrium state, but the domain-averaged precipitation rate is 3.4 mm day^{-1}, domain-averaged precipitable water is 41 mm, and maximum updraft speeds are 15–25 m s^{-1}, all of which are realistic for tropical oceanic observations (Stephens 1990; Heymsfield et al. 2010; Adler et al. 2012).

b. *Cluster and linear systems and sensitivity experiments*

The two convective systems identified from RCE-BASE (Fig. 1), a cluster system and a linear system, are simulated at higher resolution. These two systems differ in several respects, which are demonstrated later but summarized here. One system's convective cells are organized in a cluster-like manner, while the other is more linearly oriented, as suggested by their respective names. Another difference is their propagation direction: the cluster system propagates in the negative x direction as it intensifies (and then switches propagation direction as it decays), while the linear system propagates in the positive x direction. Additionally, the linear system is shorter lived but more intense than the cluster system. By simulating two convective systems with different characteristics, we can assess whether the role of cold pools is robust across different organizational types.

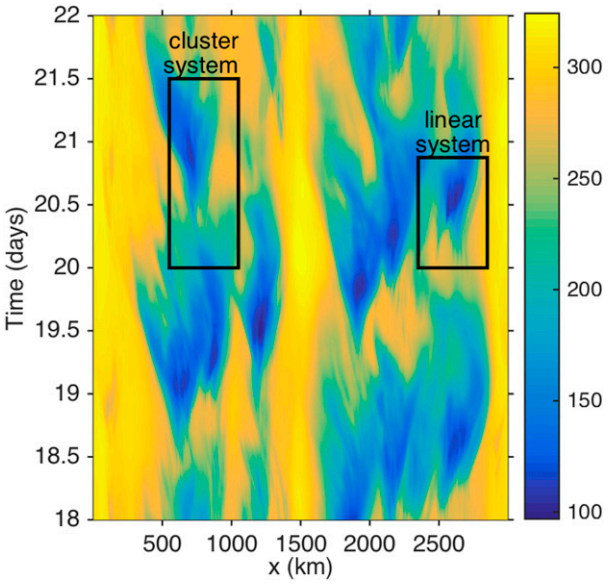

FIG. 1. Hovmöller diagram of zonally averaged OLR at model top in simulation RCE-BASE. The black boxes show the zonal extents and durations of the cluster and linear system high-resolution simulations.

Two nested control simulations were performed: control cluster (CTL-CLST) and control linear (CTL-LIN). Both control (CTL) simulations used 250-m horizontal grid spacing, 30-m (near surface) vertical grid spacing stretched to 250 m aloft, and a 2.5-s time step. The finer grid spacings permit better representation of the turbulence and cold pool characteristics (Bryan et al. 2003; Grant and van den Heever 2016). Both CTL runs extended 500 km in the zonal (x) direction to capture the entire moist band that each system lives within and 200 km in the meridional (y) direction to match that of the RCE-BASE simulation, giving a total of 2000 × 797 × 128 grid points for each domain. The meridional lateral boundary conditions were kept periodic, but the zonal boundary conditions were changed to open radiative (Klemp and Wilhelmson 1978) and nudged with the RAMS output from the RCE-BASE simulation

using a nudging time scale of 15 min. Each CTL simulation was initialized from the day 20 instantaneous RCE-BASE fields interpolated onto the higher-resolution grid. The only difference between the two CTL simulations was their x position in the RCE-BASE run and the length of integration time. CTL-CLST was initialized from $x = 550$ to $x = 1050$ km in RCE-BASE and run for 36 h, as shown by the left box in Fig. 1, while CTL-LIN was initialized from $x = 2350$ to $x = 2850$ km and run for 21 h (right box in Fig. 1). In each case, the total run time captures the intensifying through dissipating stage of the system. Model output was stored every 10 min. From here on, "hour 0" of the higher-resolution simulations will refer to the initialization time, corresponding to day 20 of RCE-BASE.

To investigate the role of cold pools in the tropical convective systems, we altered the cold pool strengths by changing hydrometeor evaporation rates below cloud base (~330 m AGL, where the second derivative of the domain- and time-mean cloud water mixing ratio profile is maximized in the CTL simulations, i.e., where there is the most curvature in the mean cloud water profile). Similar cold pool modification methods have been used in several previous studies (e.g., Crook and Moncrieff 1988; Jeevanjee and Romps 2013), although most, if not all, prior studies modify evaporation over a greater depth than just the subcloud layer. We modified evaporation only below cloud base in order to avoid altering other aspects of the convection (such as entrainment rates and gravity waves), which would complicate the interpretation of the cold pools' roles. Sensitivity experiments were conducted with the modified evaporation rates by restarting the CTL simulation at hour 5 for the cluster system and hour 3 for the linear system, both of which are 5 h before the main analysis period (hours 10–20 for the cluster system and hours 8–16 for the linear system, when the propagation speed is well defined; see section 3b). Two of the sensitivity experiments were called evaporation-off cluster (EOFF-CLST) and evaporation-off linear (EOFF-LIN). In these tests, evaporation below cloud base was shut off completely by setting water vapor diffusivity to 0.[1] This is the most we can weaken the cold pools without also changing evaporation above cloud base.

Because the cluster system showed a larger response in the EOFF experiment than did the linear system (as shown in the next section), two additional sensitivity experiments were also performed for the cluster system: E1/2-CLST, in which water vapor diffusivity was reduced by a factor of 5, resulting in evaporation rates that are approximately halved, and E2X-CLST, in which water vapor diffusivity was increased by a factor of 5, resulting in an approximate doubling of evaporation rates and stronger cold pools. In summary, six high-resolution simulations were performed: CTL-CLST, EOFF-CLST, E1/2-CLST, E2X-CLST, CTL-LIN, and EOFF-LIN. E2X-CLST is the only sensitivity test in which cold pools were strengthened; in all other sensitivity tests, the cold pools were weakened.

3. Results

a. Convection intensity

Our method to weaken the cold pools by preventing evaporation only below cloud base is effective, especially in the cluster system, despite the shallow depth of the subcloud layer (Fig. 2). The method is effective because the origin of most downdraft air in weakly sheared tropical maritime systems is close to cloud base (e.g., Moncrieff and Miller 1976; Torri and Kuang 2016), which we confirmed via PDFs of moist static energy (not shown). The signature of many of the small, individual cold pools ahead of the main system have disappeared in the density potential temperature θ_ρ (Emanuel 1994) fields in the EOFF simulations (e.g., Figs. 2a,c from $x = 50$ to 150 km and Figs. 2e,g from $x = 280$ to 350 km), suggesting those small cold pools in CTL are largely created by evaporation in the subcloud layer. The average near-surface θ'_ρ values (relative to the domain-mean θ_ρ of each high-resolution grid) in the regions of strongest cold pools reach −0.55 K in CTL-CLST and −1.5 K in CTL-LIN but only reach −0.05 K in EOFF-CLST and −0.85 K in EOFF-LIN.

If cold pools are initiating and/or helping to maintain convection in the two systems, we would expect the convective systems to be weaker in the EOFF simulations than in the CTL simulations, as hypothesized. However, the OLR fields in Fig. 2 suggest that the opposite is true. In the cluster system, low OLR regions cover more area in EOFF than in CTL, indicating wider coverage of cold cloud tops (Figs. 2b,d). In the linear system, differences between the OLR fields are subtle, though individual convective elements appear slightly wider with colder cloud tops in EOFF (Figs. 2f,h). Differences in OLR

[1] In the RAMS microphysics, condensation and evaporation are calculated by one routine that simultaneously updates water vapor mixing ratio, hydrometeor mixing ratios and internal energies, and air temperature following the analytical formulas of Walko et al. (2000). Evaporation rates were therefore modified as follows: First, the condensation/evaporation code was allowed to run as normal, and grid points below cloud base that underwent evaporation were flagged. For these grid points, condensation/evaporation was recalculated with a modified value of water vapor diffusivity. This method alters both the mass transfer of water between vapor and condensed phases and the associated latent heating, and it also allows hydrometeor mixing ratios and internal energies, water vapor mixing ratio, and air temperature to remain self-consistent.

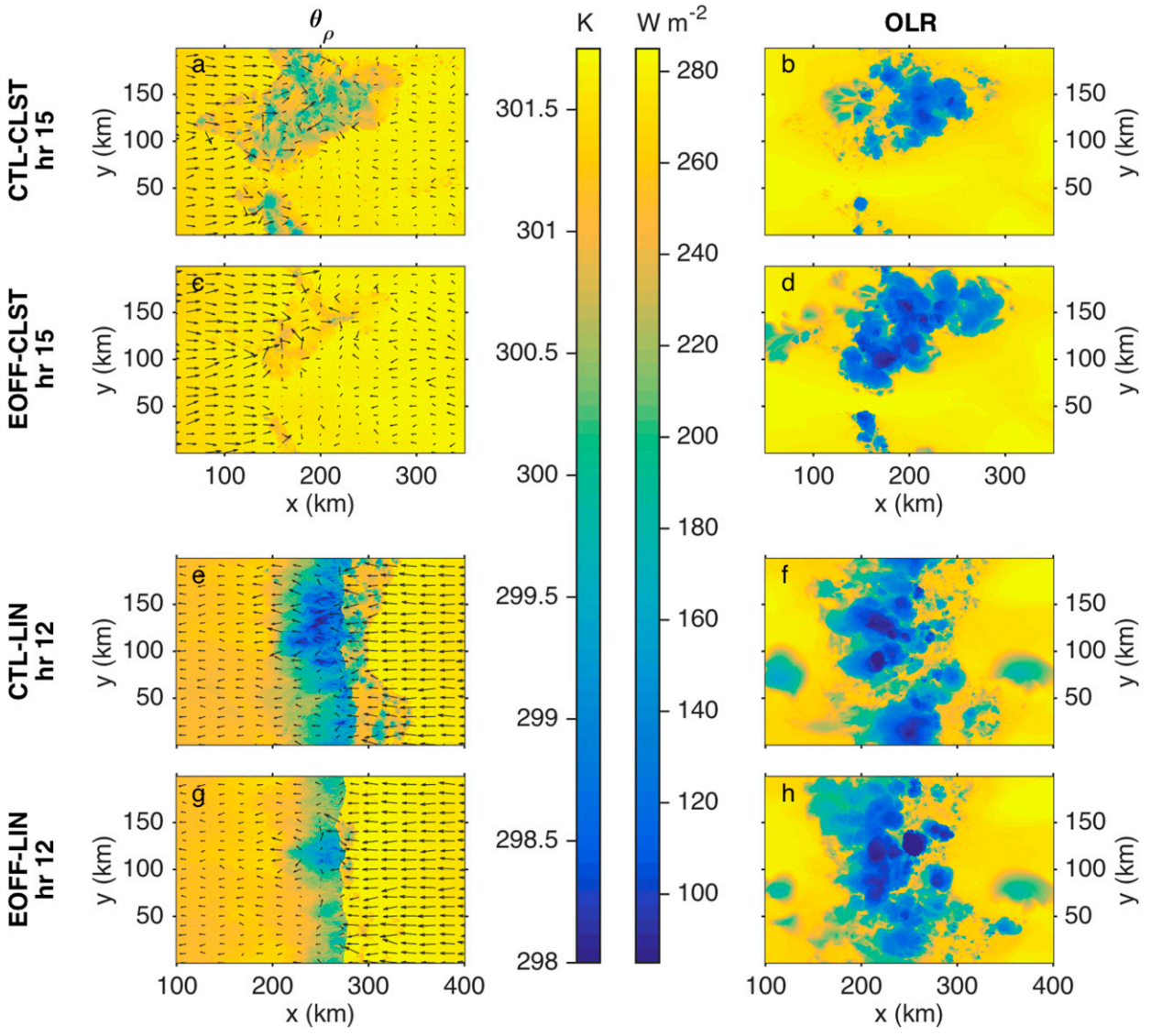

FIG. 2. Instantaneous plan views of (a),(c),(e),(g) θ_ρ and system-relative wind vectors (see section 3b for propagation speeds) at the lowest model level (15 m AGL); and (b),(d),(f),(h) OLR. Simulations (a),(b) CTL-CLST and (c),(d) EOFF-CLST are shown at hour 15 of the high-resolution simulations, and simulations (e),(f) CTL-LIN and (g),(h) EOFF-LIN are shown at hour 12.

between CTL-LIN and EOFF-LIN are more obvious at later hours (not shown).

The surprising result that convection is more intense in EOFF than in CTL suggested by the snapshots in Fig. 2 is corroborated by analysis of multiple measures of convective intensity. One such measure is mean precipitation rate, which is noticeably greater in EOFF compared to CTL, particularly when the precipitation rate is decaying (Fig. 3a). The corresponding domain- and time-mean precipitation rate (and therefore also the total accumulated precipitation) increases by 7%–17% in the EOFF simulations (Table 1). The precipitation-rate probability distributions in the four CTL and EOFF simulations (Fig. 4) tell a similar story as the average precipitation rates. For instance, the frequency of occurrence of moderate, 40–80 mm h^{-1} precipitation rates increases by about 25% in EOFF for the linear system and by 50%–500% for the cluster system (Fig. 4b).

Precipitation is not a perfect measure of convective intensity for these experiments because when subcloud evaporation is reduced, more water will reach the surface as precipitation, all else being equal. However, the precipitation differences between CTL and EOFF are also associated with changes in OLR and therefore in cloud-top temperatures (Fig. 3b). OLR is lower on average in the EOFF simulations than in the corresponding CTL

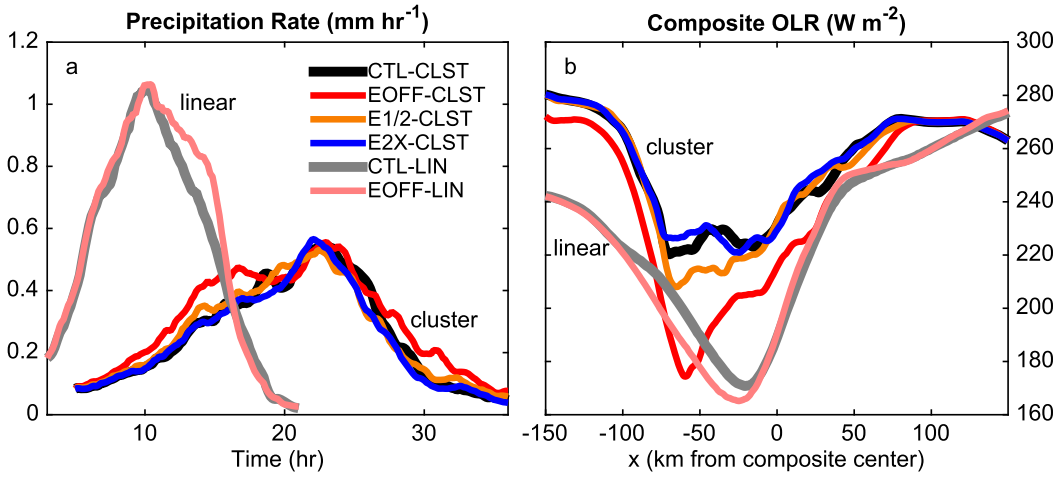

FIG. 3. (a) Time series of domain-averaged precipitation rate for all six high-resolution simulations as shown in the legend. (b) Composite OLR for the same six simulations. Composites were created by following the system at its propagation speed (see section 3b) and averaging meridionally and temporally over hours 10–20 for the cluster system and hours 8–16 for the linear system.

simulations, indicating colder cloud tops associated with more intense and/or more widespread deep convection. Such OLR differences suggest that the precipitation increase in the EOFF simulations is primarily due to increased convective vigor and not due to the reduced subcloud evaporation.

The two additional sensitivity tests for the cluster system (E1/2 and E2X) follow the same trend as the EOFF simulations (Fig. 3 and Table 1): precipitation increases in E1/2 when cold pools are weakened by the reduced evaporation rates, as in EOFF, while precipitation decreases in E2X when cold pools are strengthened by faster evaporation rates; OLR changes accordingly. The magnitude of the difference is much smaller in E1/2 (E2X) than in EOFF, despite the 1/2 (2) factor change in evaporation rate, all else being equal. However, not all else is equal: when cold pools are weakened by slower evaporation rates in E1/2, the cold pools become warmer and drier and therefore have lower relative humidity, which acts to increase the evaporation rates again, thereby resulting in a negative feedback on the initial decrease in evaporation rate. The negative feedback similarly exists in E2X. This feedback acts to keep the E1/2 and E2X cold pool properties and system intensity similar to those of the CTL run. The feedback does not exist in the EOFF simulations since the evaporation cannot respond to changes in relative humidity in EOFF. This result may indicate that, in reality, cold pools in the tropics may be fairly insensitive to factors such as drop size distributions or surface fluxes that could otherwise perturb cold pool strengths. Given the small changes in E1/2 and E2X compared to CTL, the remaining analysis will focus only on the CTL and EOFF simulations.

TABLE 1. Domain- and time-averaged precipitation rate in the CTL simulations and percentage differences from CTL for the sensitivity simulations, averaged over the duration of the sensitivity simulations (hours 5–36 for the cluster system and hours 3–21 for the linear system).

Simulation	Precipitation rate
CTL-CLST	0.26 mm h^{-1}
EOFF-CLST	+16.96%
E1/2-CLST	+1.51%
E2X-CLST	−4.01%
CTL-LIN	0.54 mm h^{-1}
EOFF-LIN	+6.93%

The final measure of convective intensity we examine here is the updraft strength. The 95th percentile of updraft speeds do not exceed 5 m s^{-1}, while the fastest updraft speeds are between 15 and 25 m s^{-1} for both systems (Figs. 5a,c), which are in the range of observations for tropical oceanic convection (LeMone and Zipser 1980; Lucas et al. 1994; Heymsfield et al. 2010; Varble et al. 2014; Schumacher et al. 2015). In the cluster system, EOFF has up to 1 m s^{-1} stronger vertical velocities above 4 km AGL (Fig. 5b), and between 6 and 8 km AGL, the relative increase in updraft speed in EOFF compared to CTL exceeds 20% for the 90th–99th percentiles. EOFF-LIN also has stronger mid- and upper-troposphere updraft speeds than CTL-LIN, although the magnitude of the differences is slightly smaller (Fig. 5d). The increases in updraft speed for both

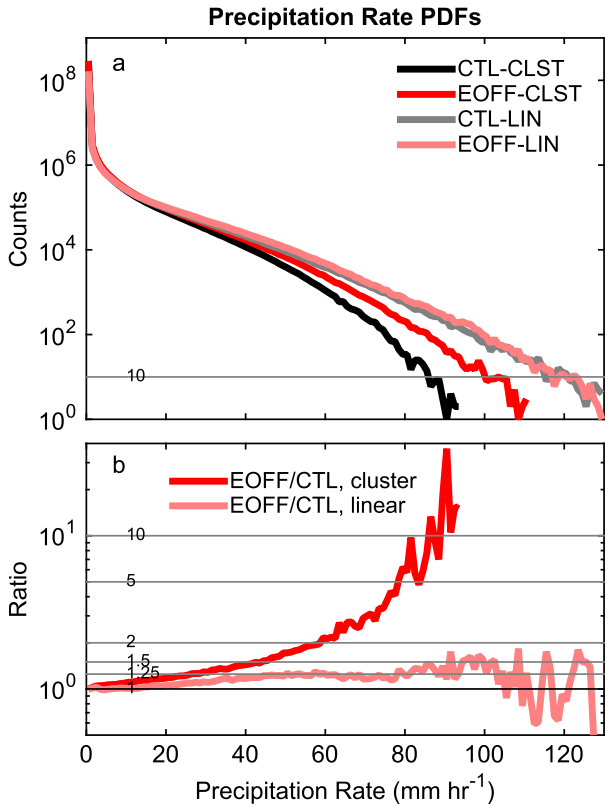

FIG. 4. (a) PDFs of precipitation rate for both CTL and EOFF simulation sets as indicated in the legend. The precipitation-rate bin width is 1 mm h^{-1}. Counts are accumulated over hours 10–20 for the cluster system and hours 8–16 for the linear system. (b) Ratio of precipitation-rate bin counts in EOFF to CTL.

EOFF cases are consistent with the increase in precipitation and reduction in OLR and suggest an overall increase in the mesoscale upward circulation. However, interesting trends appear for the strongest updraft speeds over the lowest 4 km, which are associated with the initiation of a small number of intense, convective-scale updrafts by cold pools. For the cluster system, the strongest updrafts are weaker in the EOFF case below 2 km AGL (for the 97.5th percentile) and below 4 km AGL (for the 99.9th percentile). However, for the linear system, the updrafts are stronger at all depths in the EOFF case except between 3 and 6 km AGL, where they are weaker for the 99.9th percentile. These differences between the two systems are presumably related to the differences in low-level inflow to the two systems and their convective-scale initiation, which is discussed further in section 3b.

In summary, we have analyzed various metrics for convective intensity and have shown that when cold pools are weakened, the convection becomes more intense. We hypothesize that cold pool air becomes incorporated into the updrafts and its initial negative buoyancy reduces the convective intensity. This idea is explored further in section 3c. These results suggest that the cold pools are not playing critical roles in convective initiation and that mechanisms other than cold pools are more important for initiating and maintaining convection, such as gravity waves (e.g., Balaji and Clark 1988; Pandya and Durran 1996; Lane and Reeder 2001; Lac et al. 2002).

b. *Propagation and mesoscale structure*

Given the large differences seen in the cold pools themselves and in the convective intensity, it is natural to next ask, Are the propagation speeds different and/or is the mesoscale structure altered in the EOFF simulations? If the cold pools define the propagation speed of the systems (e.g., as in LM15), then we would expect to find slower propagation in the EOFF simulations than in the CTL simulations, as we originally hypothesized. Additionally, if RKW theory is applicable to the linear systems, then differences in the mesoscale structure (e.g., system tilt) and maintenance should arise because of the weakened cold pools.

We can answer whether the cold pools are playing a role in the propagation speeds by examining Hovmöller diagrams of condensed water path (Fig. 6). The cluster system slowly propagates in the negative x direction at about 1 m s^{-1} between hours 10 and 20, when the propagation speed is clearly defined (Fig. 6a), while the linear system propagates more quickly in the positive x direction at about 6 m s^{-1} (Fig. 6c). Despite the fact that the EOFF simulations have weaker cold pools, we see by comparing the slopes of the black and red contour overlays in Fig. 6 that the propagation speeds are not distinguishably different between CTL and EOFF for either system. The lifetimes of both systems and the time at which the cluster system switches propagation direction are also not affected by the changes to the cold pools. We therefore conclude that the cold pools *do not* play the dominant role in determining propagation speeds, nor do they significantly impact the lifetimes and evolution of the systems.

To determine whether the cold pools influence the mesoscale flow patterns and structure of the systems, we compare composite cross sections for CTL and EOFF, beginning first with the cluster system.[2] We define the

[2] Despite the cluster-like appearance of this system in the θ_ρ and OLR fields, the predominant flow is zonal and fairly meridionally symmetric (see Fig. 2) because of the channel configuration and cyclic boundary conditions of the RCE-BASE run, which justifies a simple meridional averaging method.

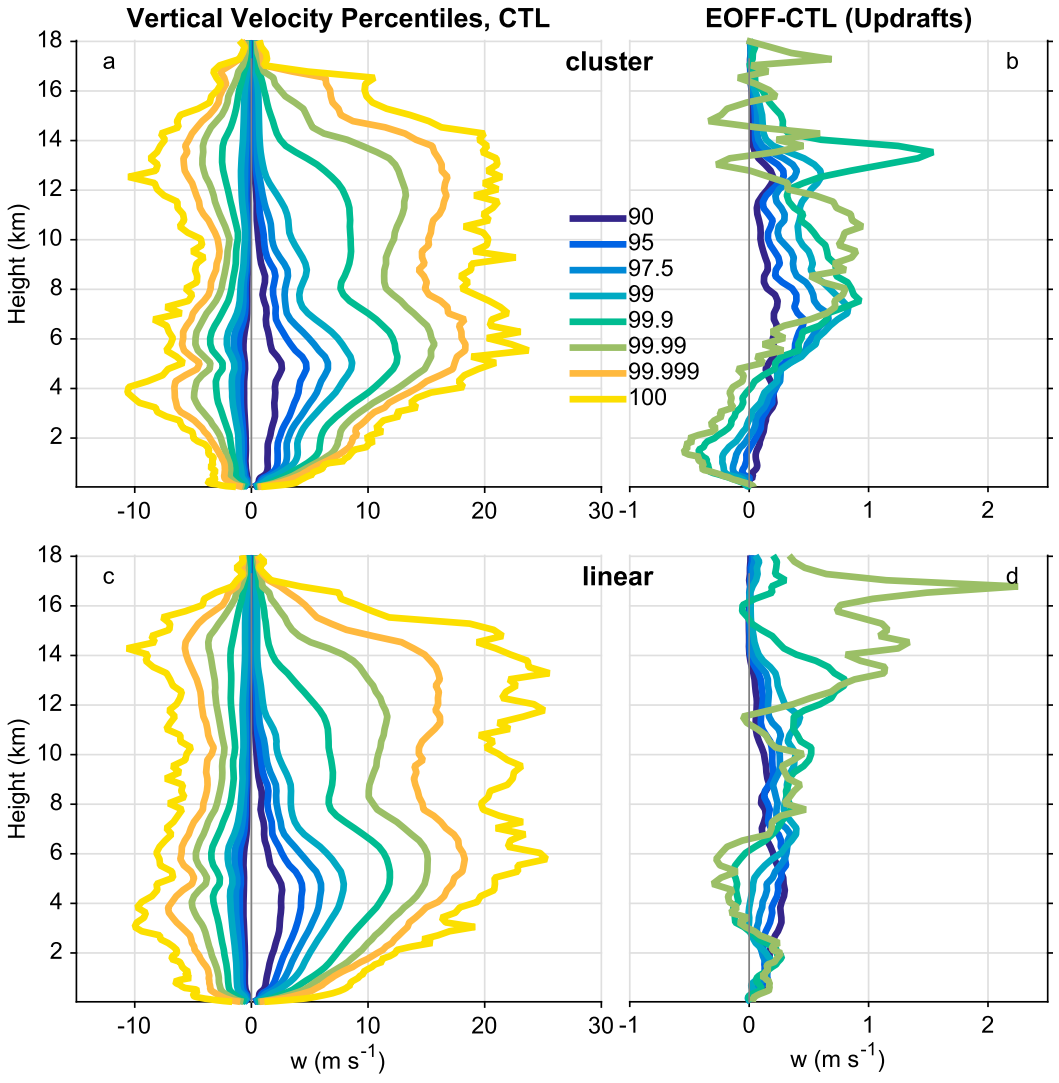

FIG. 5. (left) Percentiles of vertical velocity for $|w| \geq 0.1\ \mathrm{m\ s^{-1}}$ as a function of height in (a) CTL-CLST over hours 10–20 and (c) CTL-LIN over hours 8–16. (right) Differences between EOFF and CTL for upward vertical velocity percentiles ($w \geq 0.1\ \mathrm{m\ s^{-1}}$) in (b) the cluster system and (d) the linear system. The 99.999th- and 100th-percentile differences are not shown because of noise.

system-relative streamlines in the same way as LM15. Several notable features of the CTL-CLST structure are apparent in Figs. 7a and 7c. The full-troposphere view of the streamlines shows several flow branches: front-to-rear jump updrafts originating primarily at three different levels (near the surface and at 4 and 7.5 km AGL), an overturning circulation above 9 km AGL (between $x = -150$ and -50 km), and a low-level ascending and overturning circulation at the back of the system (between $x = -25$ and 150 km). A mesoscale downdraft does not exist, the boundary layer relative humidity is between 80% and 90%, and convective inhibition in the inflow environment is small along with moderate CAPE (Fig. 9), similar to the system studied in ML15. The low-level shear ahead of (to the left of) the cluster system is in the negative x direction (Fig. 10a), so it propagates downshear but tilts upshear.

The composite cold pool in CTL-CLST has a minimum θ'_ρ of -0.55 K and a theoretical propagation speed[3] of $3\ \mathrm{m\ s^{-1}}$. These weak values are consistent with the high humidity in the boundary layer (Figs. 7a and 9). In EOFF, the minimum θ'_ρ is only -0.05 K, and the

[3] Theoretical cold pool propagation speed C is calculated as $C^2 = 2\int_0^H -B\,dz$ (Benjamin 1968), where H is the top of the cold pool, taken to be 500 m AGL (see Figs. 7 and 8) and $B = g\theta'_\rho/\overline{\theta}_\rho$ is the buoyancy.

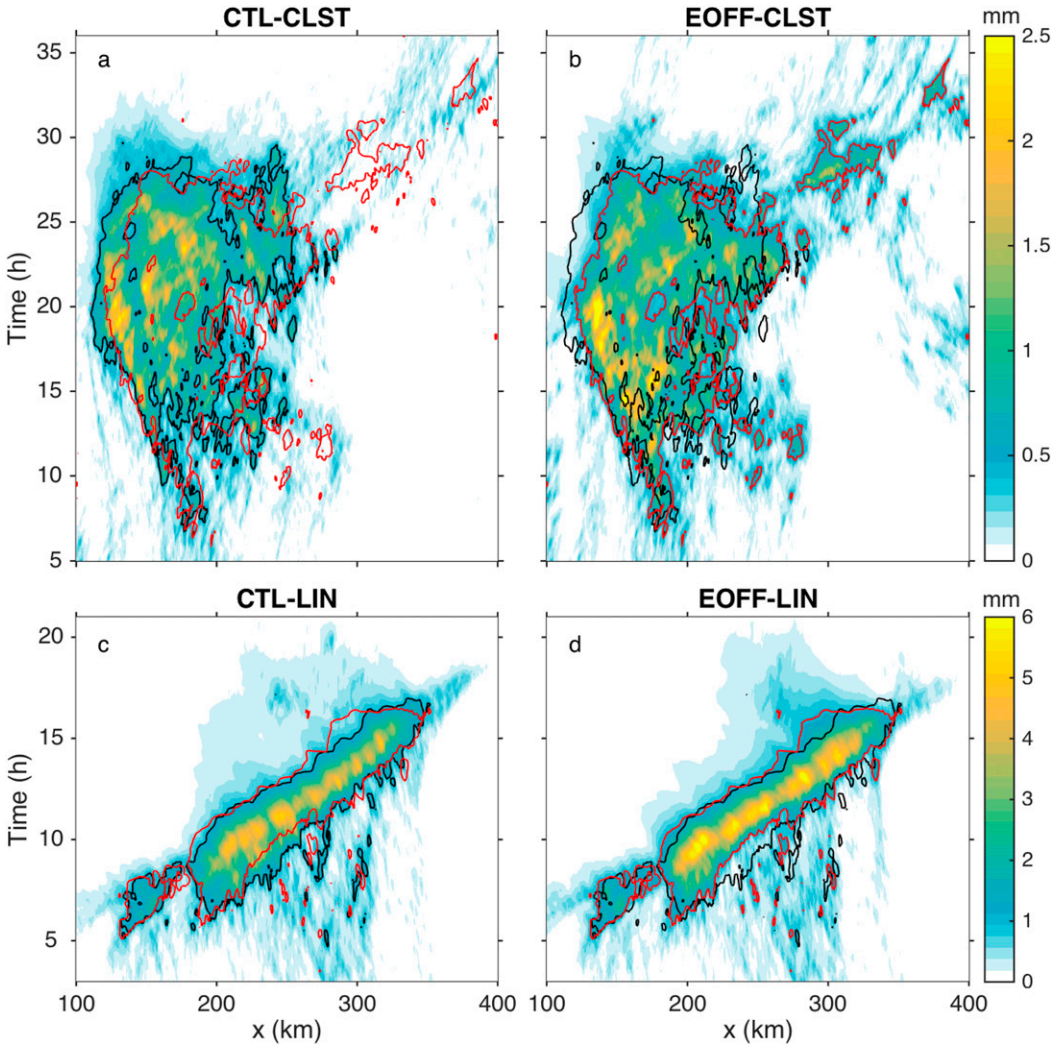

FIG. 6. Hovmöller diagrams of meridionally averaged condensed water path (mm) in (a) CTL-CLST, (b) EOFF-CLST, (c) CTL-LIN, and (d) EOFF-LIN. To aid comparison, the 0.5-mm contour is shown in black for CTL-CLST and in red for EOFF-CLST in (a) and (b), while the 1-mm contour is shown in black for CTL-LIN and in red for EOFF-LIN in (c) and (d).

theoretical speed is reduced to $1\,\mathrm{m\,s^{-1}}$. Despite these substantial cold pool changes, the general mesoscale structure is nearly unchanged in EOFF compared to CTL. There are only small differences in the streamlines, such as a stronger upper-level overturning circulation in EOFF and slightly steeper streamlines in CTL between 1 and 3 km AGL above the leading edge of the composite cold pool (around $x = -75$ km). The steeper low-level streamlines result in a sharper horizontal gradient of condensate mixing ratios (Fig. 7c). These structures are consistent with some convective-scale initiation by the cold pool near the surface and the larger values of the most intense low-level updrafts in CTL-CLST compared to EOFF-CLST (Fig. 5b). In CTL, low-level ascending streamlines originating within the subcloud layer pass through the composite cold pool and falling precipitation (Fig. 7c). This indicates that, from the viewpoint of the mesoscale flow, the low-level inflow to the CTL-CLST system acquires negative buoyancy through evaporative cooling in the subcloud layer, which lends support to the hypothesis that the evaporation that forms cold pools is actually having a detrimental effect on the intensity of convection by reducing the buoyancy of the inflow air.

The linear system exhibits many similar mesoscale features to the cluster system (Fig. 8) as it forms in a very similar thermodynamic environment (Fig. 9). For instance, the system has ascending front-to-rear flow and a

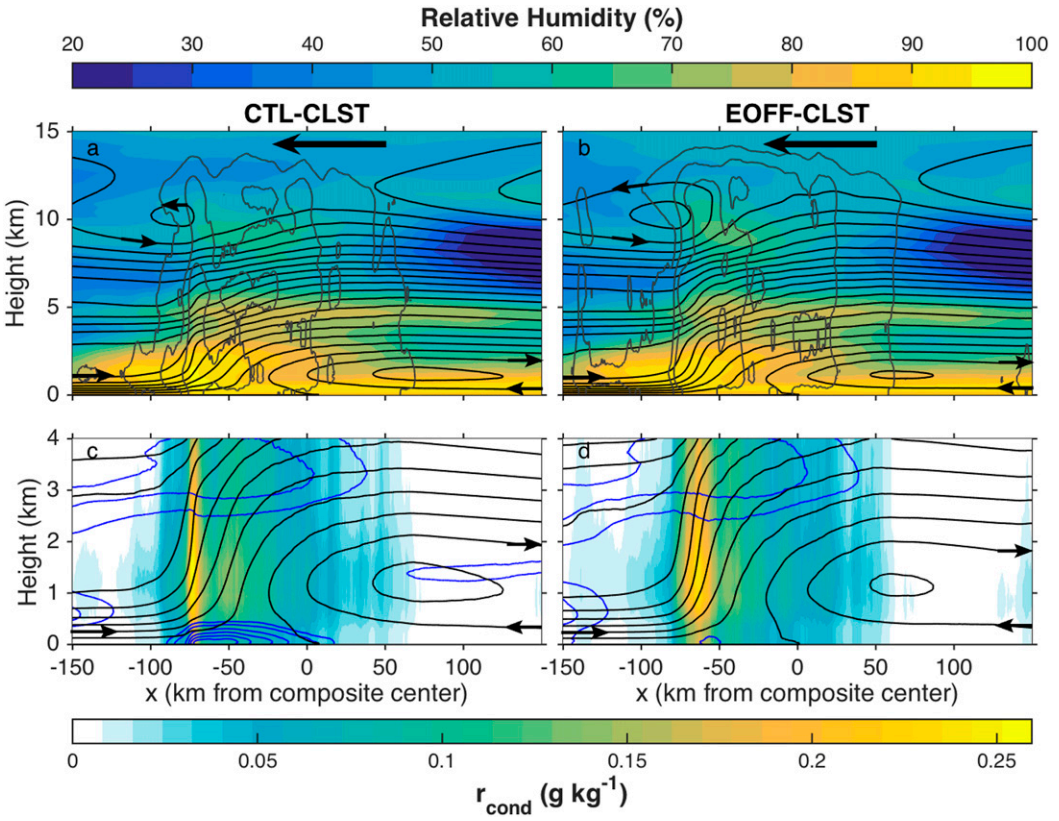

FIG. 7. (a),(b) Composite cross sections of relative humidity with respect to liquid water (shaded), total condensate mixing ratio (0.01, 0.05, 0.1, and 0.5 g kg^{-1}; gray contours), and system-relative streamlines (black contours) calculated from the composite system-relative zonal wind. (c),(d) Composite cross sections of total condensate mixing ratio (shaded), negative values of θ'_ρ (blue contours every -0.1 K, plus -0.05 K), and system-relative streamlines (black contours), zoomed in on the lowest 4 km AGL. Composites were created by following each system at its propagation speed (-1 m s^{-1} for the cluster system) between hours 10 and 20 and then averaging meridionally and temporally. Note that streamlines flow from left to right at all levels except between $x = -25$ and 150 km over the lowest 1 km AGL and above approximately 12 km AGL, where they flow from right to left. The small arrows indicate the direction of flow along streamlines, while the thick arrows at the top indicate the system's propagation direction.

jump updraft since the streamlines end up at a higher altitude than they originated, and the system lacks a mesoscale downdraft. The low-level shear ahead of (to the right of) the system is in the positive x direction (Fig. 10b), so it also propagates downshear and tilts upshear, as in the cluster system. It is worth noting that the linear system's propagation speed and its environmental shear compare well with observed shear-perpendicular lines documented in LeMone et al. (1998) and Johnson et al. (2005). The composite cold pool in CTL-LIN is stronger than in CTL-CLST: its minimum θ'_ρ is -1.5 K and theoretical speed is 5.7 m s^{-1}. In EOFF-LIN, the minimum θ'_ρ has been reduced by nearly half, and the theoretical speed is 12% lower. Both CTL-LIN and EOFF-LIN do show small regions of stagnation within the composite cold pool (indicated by the circular streamline), and the horizontal maps (Fig. 2) show a well-defined leading edge and system-relative flow toward the front of the cold pool, as might be expected in association with the presence of a density current. However, despite the changes to the cold pool structure from CTL-LIN to EOFF-LIN, there are nearly indistinguishable changes in mesoscale structure, which indicates that the mesoscale behavior of these systems is not sensitive to the details of the cold pool. Yet, as shown earlier, the EOFF case has stronger updrafts throughout the depth of the convection and more intense precipitation.

The increase in intensity of the linear system with weaker cold pools could potentially be explained by two important changes in the composite mesoscale structure of the system. First, the intensity response appears consistent with RKW theory: Δu over the lowest 2 km is less than 2 m s^{-1} for both the CTL and EOFF systems (Fig. 10b),

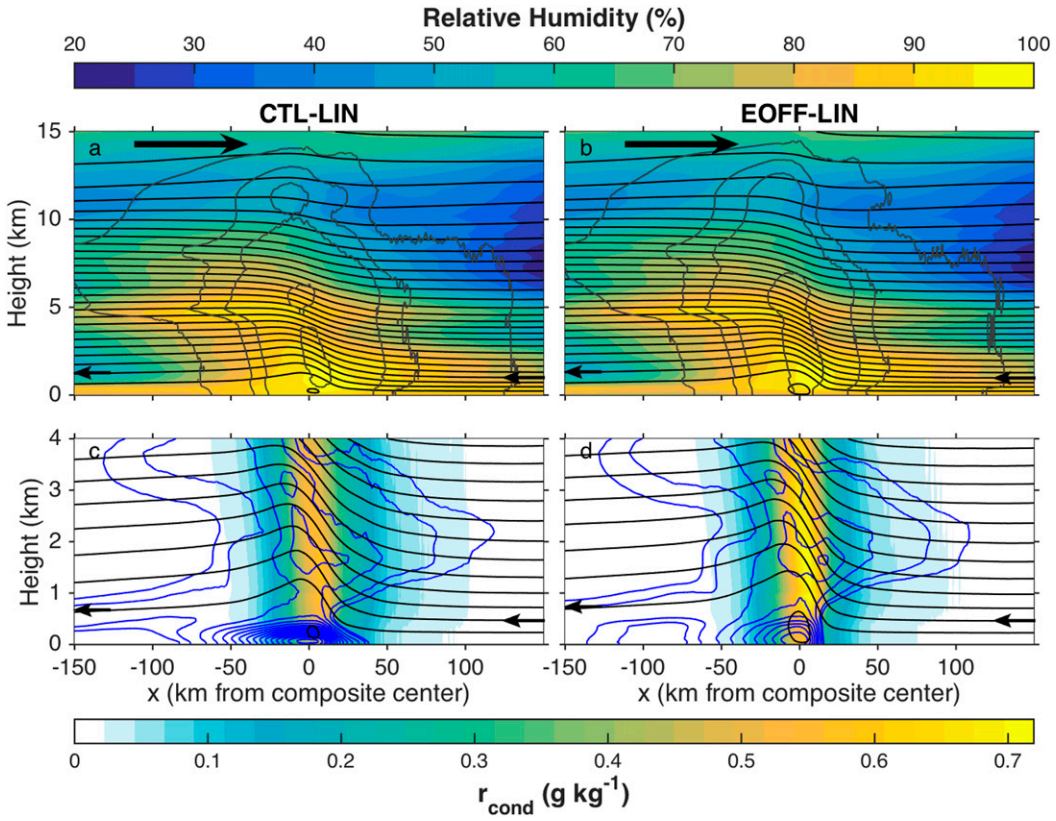

FIG. 8. As in Fig. 7, but for the linear system: for construction of the composites, each system was followed at its propagation speed of $+6\,\mathrm{m\,s^{-1}}$ between hours 8 and 16. Note that streamlines flow from right to left at all levels as indicated by the small arrows in the bottom corners of each panel. The thick arrows at the top indicate the system's propagation direction.

and hence $C/\Delta u$, which equals 3.4 in CTL and 3.0 in EOFF, is closer to 1 in EOFF and therefore in a more optimal state, albeit within relatively weak shear. Indeed, as expected, the streamlines are slightly steeper in Fig. 8d than in Fig. 8c on a local, convective scale (at low levels near the composite cold pool). Second, the leading precipitation and evaporation in CTL-LIN produces a cold pool that protrudes about 25 km ahead of EOFF-LIN's cold pool. As in the cluster system, the low-level inflow passes through this protruding cold pool in CTL-LIN. This flow pattern bears some resemblance to the midlatitude, front-fed, leading stratiform convective systems simulated by Parker and Johnson (2004) except that, here, the leading precipitation is not stratiform in nature nor advected from the convective region but rather is formed by congestus clouds ahead of the main convective line (e.g., see Fig. 2). The inflow through the composite cold pool, along with the evaporation of the leading precipitation, reduces the buoyancy of the inflow. Hence, the low-level inflow in EOFF-LIN does not experience the detrimental effects of the protruding cold pool and evaporation as in CTL-LIN, and the system is more intense as a result.

With the exception of the small region of stagnation in the cold pool, the linear system is strictly propagating; that is, there is no steering level, and hence, streamlines pass through the system from right to left at all levels, and there is no evidence of a mesoscale downdraft. The system appears to propagate in a wave-like manner, which is also consistent with the cold pools' weak influence on the mesoscale features. Perhaps most importantly, both CTL-LIN and EOFF-LIN have nearly identical propagation speeds, regardless of cold pool strength. Thus, despite some local, convective-scale features of the linear system being consistent with RKW theory, the overall behavior of the linear system and its mesoscale structure suggests that some other mechanism is responsible for the system propagation and longevity.

c. *The role of cold pools in convective intensity*

We hypothesize based on the results of section 3a that the presence of the cold pools weakens convective intensity through the impacts of negative buoyancy in the subcloud layer, implying that some of the rising updraft

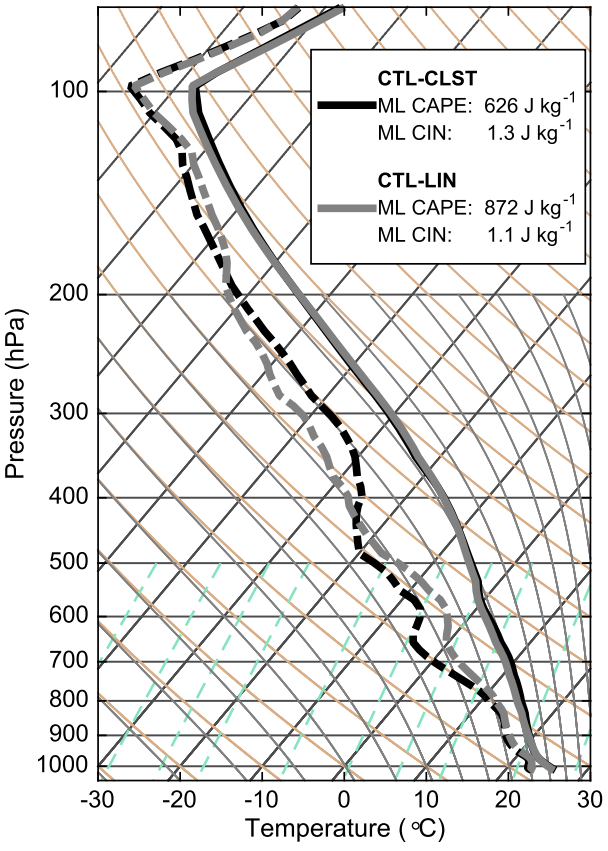

FIG. 9. Skew T–log$p$ plot of temperature (solid lines) and dewpoint temperature (dashed lines) for the composite inflow environment of both CTL systems as indicated in the legend. In the composite frameworks, the inflow environments were defined to be similar distances ahead of the convective systems, specifically, from $x = -150$ to $x = -100$ km for CTL-CLST and from $x = 50$ to $x = 100$ km for CTL-LIN. Mixed-layer CAPE and CIN calculations are shown in the legend, where the mixed-layer depth was assumed to be 500 m.

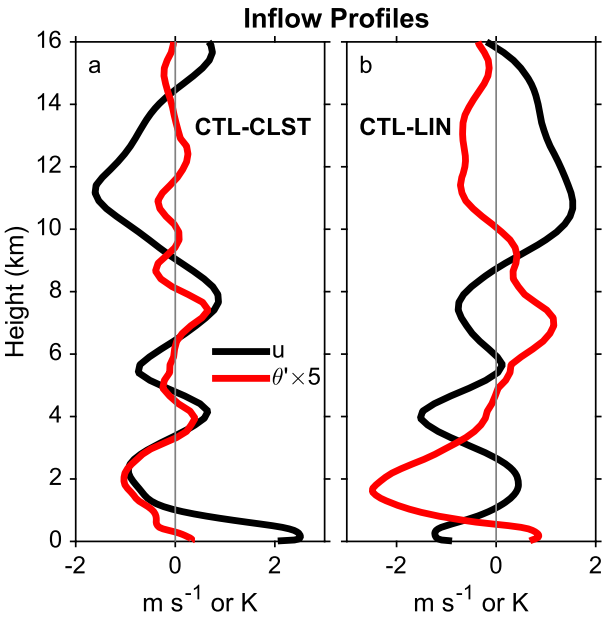

FIG. 10. (a) Composite inflow environment profiles of u and θ' (defined relative to the mean θ at each altitude) for the CTL-CLST system. The θ' profile is multiplied by a factor of 5 as indicated in the legend so that its magnitudes are similar to the wind speed. (b) As in (a), but for the CTL-LIN system. The inflow environments were defined as in Fig. 9.

air originates from within the cold pools. While at first this feels counterintuitive, it is well known that cold pools are detrimental to unorganized convection (Byers and Braham 1949) because the cold pools can undercut the parent updrafts. Additionally, prior studies of unorganized tropical convection have suggested that updrafts do transport some air from the cold pools (e.g., Tompkins 2001; Torri et al. 2015). We investigated how much cold pool air is transported aloft by the updrafts in these two convective systems through additional experiments in which passive tracers were initialized within the CTL and EOFF cold pools. Eighteen different tracers were initialized at the middle of the analysis periods when precipitation differences are large (hour 15 for the cluster systems and at hour 12 for the linear systems) and were integrated for 2 h. The tracer initialization regions, which are visually summarized for the two CTL systems in Figs. 11a–d, were determined as follows. Tracers 1–9 were initialized in regions where $\theta'_\rho \le -0.5$ K and tracers 10–18 were initialized where $\theta'_\rho \le -1$ K, thereby allowing us to evaluate whether the amount of air that is transported by updrafts depends on the initial negative buoyancy. The tracers were given an initial mixing ratio of 1 kg kg^{-1} and were initialized at one of the nine lowest vertical model levels, all of which are below cloud base. Tracers 1 ($\theta'_\rho \le -0.5$ K) and 10 ($\theta'_\rho \le -1$ K) were placed closest to the surface (15 m AGL), followed by tracers 2 and 11 in the next vertical model level and so on. Tracers 9 and 18 are the highest tracers (308 m AGL) and are hence initialized closest to cloud base.

The percentage of each tracer's total mass that has been transported above 3 km AGL after 2 h is shown in Figs. 11e and 11f. The 3-km level resides above the tops of boundary layer cumuli, so tracers transported above this altitude must have been carried there by congestus or deep convective updrafts. Over 21% of the near-surface cold pool air in the cluster system and up to 17% in the linear system ends up above 3 km (tracers 1 and 2). Additionally, it is evident from Figs. 11e and 11f that more of the upward-transported cold pool air originates near the surface (tracers 1–3 and 10–12) than higher in the subcloud layer (tracers 7–9 and 16–18), although this altitude dependency is weaker in the EOFF simulations.

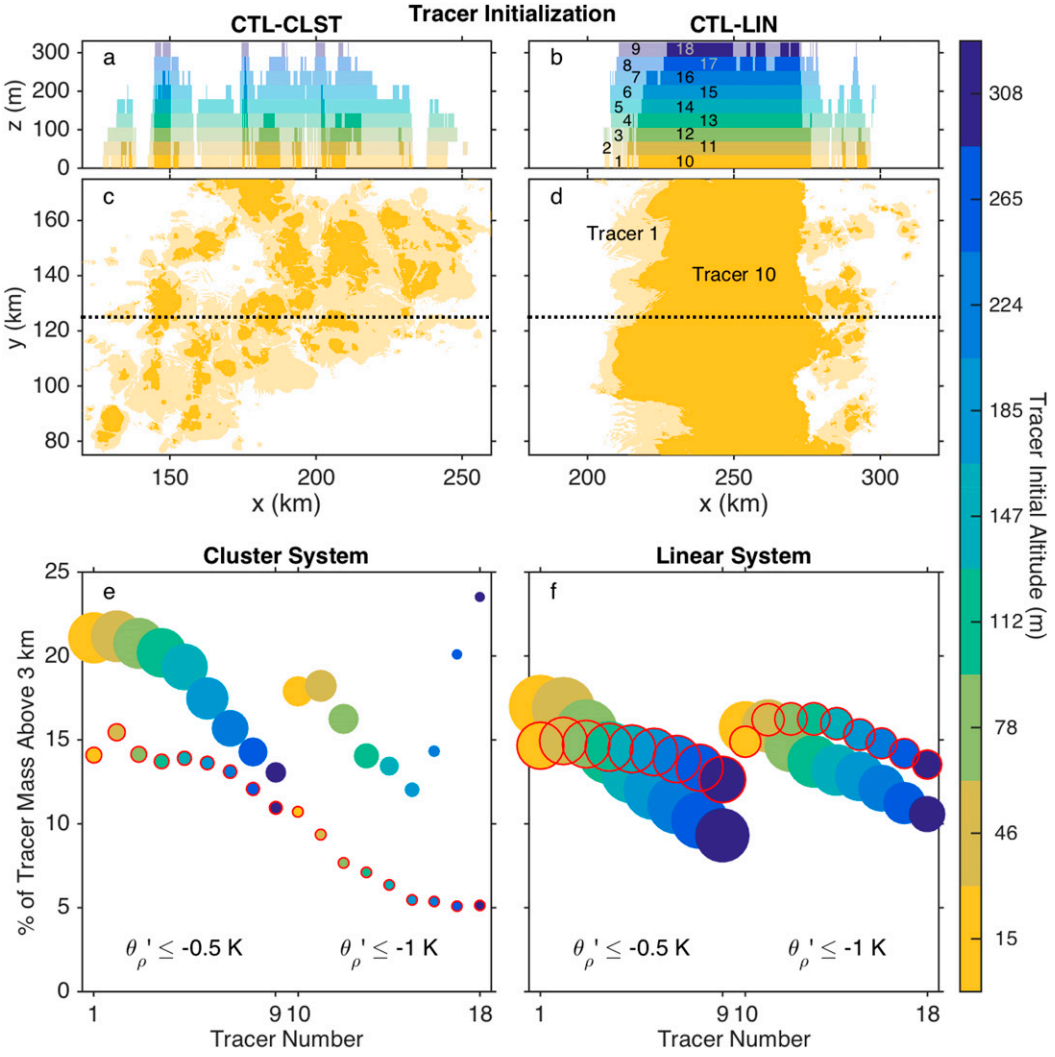

FIG. 11. (top) Cross sections through $y = 125$ km and (middle) zoomed-in plan views at 15 m, depicting tracer initialization regions in (a),(c) the CTL-CLST system at hour 15 and (b),(d) the CTL-LIN system at hour 12. Translucent (opaque) shading represents tracers 1–9 (10–18) initialized in regions where $\theta_\rho' < -0.5$ K ($\theta_\rho' < -1$ K), and the color indicates the tracer's initial altitude. Tracer numbers are labeled in (b) and (d). The dotted lines in the plan views indicate the cross-section locations. (bottom) Fraction of each cold pool tracer's initial mass that is found above 3 km AGL after 2 h of simulation time for (e) the cluster systems and (f) the linear systems. The CTL cases are shown by filled dots without an outline, and the EOFF cases are shown by red-outlined dots. The dot color indicates the tracer's initial altitude. The dot's size is proportional to the initial area percentage covered by each tracer. The largest dot represents 18.07% area coverage (CTL-LIN tracer 2), and the smallest represents 0.003% area coverage (CTL-CLST tracer 18).

One exception to this is tracers 17 and 18 in CTL-CLST, but those tracers cover a very small area of the domain. It is worth noting that none of the system-relative streamlines that pass through the composite cold pool ascend above 3 km in either system (Figs. 7c and 8c), which highlights the importance of considering the 3D structure of the cold pools and their behavior on convective scales. In the cluster system, the relative amount of upward-transported cold pool tracers is smaller in EOFF than in CTL (Fig. 11e). The EOFF-CLST tracers' initial distributions are shifted farther back in the system compared to CTL, and they are therefore less likely to ascend in convective updrafts given the mesoscale flow structure (Fig. 7). On the other hand, in the linear system, the relative amount of upward-transported cold pool air is greater in EOFF than in CTL except for the near-surface tracers (Fig. 11f). There are fewer tracers initialized toward the back of the system in EOFF-LIN

(e.g., between $x = 200$ and 240 km; see Figs. 11b,d and 2e,g), which may explain this result.

The tracer results lend support to our hypothesis that cold pools suppress convection intensity through their negative buoyancy, since a significant fraction of cold pool air is transported aloft. Several other studies have suggested similar findings (that the convection becomes more intense when cold pools are suppressed or weakened) both for tropical and for midlatitude organized systems. Liu and Moncrieff (2017, hereafter LM17) studied an idealized, shear-parallel, mei-yu front tropical system and demonstrated substantial intensification of the system when evaporation of rain was prevented. In simulations of a midlatitude mesoscale convective system, Trier et al. (2011) found that the MCS became more intense during its postsunrise reorganization when latent cooling from evaporation was removed. Our results also bear some resemblance to Schumacher (2015)'s study of an idealized nocturnal MCS. He showed that slight increases in low-level moisture led to large precipitation increases, suggesting the system processed and transported near-surface air through the convective region despite the stable boundary layer. Finally, these results are broadly consistent with boundary layer quasi-equilibrium theory (Raymond 1994, 1995), which postulates that downdrafts are responsible for reducing CAPE in the tropical boundary layer and extinguishing convection.

d. The role of gravity waves in system evolution

As we have shown that the mesoscale structure and propagation of the convective systems are mostly unaffected by changes to the cold pools, what then does govern the mesoscale features? We turn to gravity waves for the answer, which have been shown to be important regulators of tropical convective system behavior in several prior studies, particularly in low–convective inhibition environments (Mapes 1993; Shige and Satomura 2001; Liu and Moncrieff 2004; Tulich and Mapes 2008; Lane and Zhang 2011; LM15). Figure 12a shows a Hovmöller diagram of θ'_ρ at 3 km AGL in the RCE-BASE simulation. Various phase speeds are evident, but the most prominent signal propagates in the positive x direction at 15 m s^{-1}. We use linear theory for a fluid at rest, which defines the gravity wave propagation speed as $c_x = N/m = Z_{\text{trop}}N/\pi n$, where Z_{trop} is the troposphere depth (16 km), N is the Brunt–Väisälä frequency (0.0096 s^{-1}, averaged temporally and spatially in the troposphere), $2Z_{\text{trop}}/n$ is the vertical wavelength, and n is an integer number of antinodes within the troposphere. The phase speed of an $n = 3$ wave is 16.2 m s^{-1}, which closely corresponds to the main wave signal seen in Fig. 12a. Evidence of the $n = 3$ wave can also be seen in the inflow θ' profile for CTL-LIN (Fig. 10b). The $n = 3$ wave's half-vertical wavelength is 5.3 km, which is similar to the altitude of the freezing level (4.76 km). As this wave travels around the model domain, its horizontal wavelength is widened and its amplitude is reinforced by convective systems via latent cooling from melting and evaporation below the freezing level, similarly to mechanisms described in Tulich and Mapes (2008).

The negative low-level temperature anomalies associated with the $n = 3$ wave pass by near the time at which both the linear and the cluster systems are raining most intensely (indicated by the black dots in Fig. 12a) and when the cluster system begins to propagate in the positive rather than negative x direction. Several prior studies have highlighted the importance of the $n = 3$ wave in tropical convection initiation, organization, and behavior (e.g., Lane and Reeder 2001; Lane and Moncrieff 2008; Tulich and Mapes 2008; Lane and Zhang 2011; Tulich and Kiladis 2012). Specifically, the phase of the $n = 3$ wave that is characterized by low-level ascent and its associated cooling signal destabilizes the lower atmosphere and promotes convective development. The destabilization mechanism is particularly effective in low–convective inhibition environments such as these (Fig. 9). Additionally, Tulich and Mapes (2008) discussed the relevance of higher-order gravity wave modes than the $n = 3$ mode for convective system propagation. One of these modes was termed the "gust front" mode, so named for its similar propagation speed to the cold pools (8 m s^{-1}). The gust-front gravity wave mode may also be playing a role in the linear system's propagation through convective system–gravity wave coupling.

Since the high-resolution simulations utilize lateral boundary nudging from the RCE-BASE simulation, two-way interactions between the convective systems and the larger-scale waves are not permitted. To ensure that boundary nudging did not unduly constrain the evolution of the two systems, we ran the same EOFF experiment for the RCE-BASE simulation, executed as a restart from RCE-BASE at day 20 and integrated for 36 h (EOFF-BASE). The domain- and time-averaged precipitation rate in the RCE-BASE simulation (called CTL-BASE) is 0.144 mm h^{-1}. In the EOFF-BASE simulation, the mean precipitation rate increases by 8.5% over CTL-BASE, and the domain-averaged OLR (including both cloudy and clear regions) is up to 4 W m^{-2} colder in EOFF-BASE, confirming our precipitation rate and OLR results shown in section 3a. Additionally, the convective systems' propagation speeds do not change between CTL-BASE and EOFF-BASE (cf. Figs. 13a and 13b), which indicates that the systems

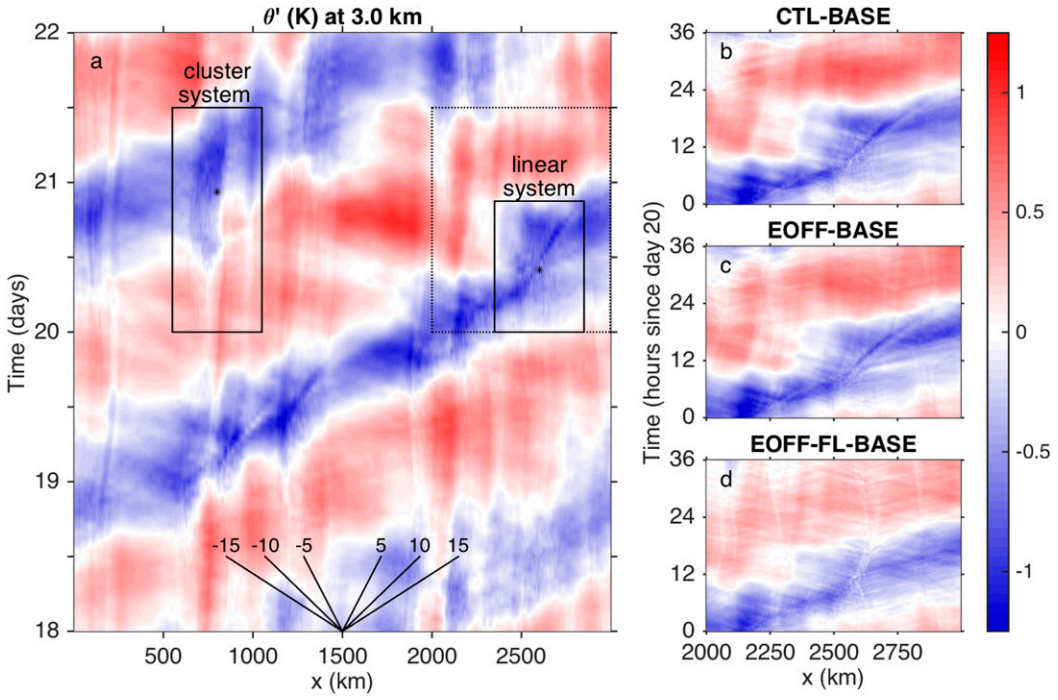

FIG. 12. Hovmöller diagrams of θ' (relative to the domain mean) at 3 km AGL for (a) the RCE-BASE simulation and (b)–(d) the BASE simulation sensitivity tests, zoomed in to the region of the linear system as outlined by the dotted box in (a); θ' is first meridionally averaged, and then the temporal average of each x column is removed. In (a), the cluster and linear systems are outlined as in Fig. 1, and the dots represent the time of maximum intensity from Fig. 3a. Black lines represent various phase speeds as labeled in the plot.

were indeed not overly constrained in the high-resolution simulations.

In a final experiment, we ran the RCE-BASE simulation with evaporation shut off everywhere below the freezing level (EOFF-FL-BASE), which alters the forcing for the $n = 3$ wave and weakens its amplitude (Figs. 12b–d). In EOFF-FL-BASE, the domain-averaged OLR decreases by more than 16 W m^{-2} compared to CTL-BASE near the end of the simulations, indicating more intense and/or more widespread deep convection. Moreover, the domain- and time-mean precipitation rate increases by 32.6%, a remarkable change and one that is consistent with that seen by LM17 in which evaporation of rain was shut off everywhere. The impact of preventing evaporation below the freezing level on the propagation of the systems is shown in Fig. 13c. Changes in the propagation speeds are clearly evident. The cluster system (around $x = 750$ km) has stopped propagating entirely, and the linear system (around $x = 2600$ km) has slowed by about a factor of 3 in its later stages. The substantial propagation change in EOFF-FL-BASE, particularly for the linear system, appears to be related to the $n = 3$ wave itself. Specifically, a slower-moving, cold signal with an amplitude of -1 K embedded within the main $n = 3$ wave begins to appear at around 10 h and $x = 2600$ km in CTL-BASE and EOFF-BASE (Figs. 12b,c), but this signal is absent in EOFF-FL-BASE (Fig. 12d). Note that this signal is not due to cold pools, since θ' is shown at 3 km, and the cold pools are only 500 m deep. The absence of this signal in EOFF-FL-BASE coincides with the beginning of the significant changes in the propagation speed (Fig. 13c), which suggests that the $n = 3$ wave may be convectively coupled to the linear system and modulates its propagation speed in CTL-BASE and EOFF-BASE. The weakening of the $n = 3$ wave in the EOFF-FL-BASE simulation may bring its amplitude below a critical threshold for the coupling to persist via destabilization.

4. Summary

RKW theory highlights the critical role of cold pools in linearly oriented convective systems. With some caveats (Evans and Doswell 2001; Stensrud et al. 2005; Coniglio et al. 2012; Alfaro 2017), this theory is widely accepted in midlatitude environments, yet the RKW authors originally postulated that it should also be applicable to tropical convective systems. A few studies have applied RKW thinking to tropical systems; some have found general agreement with the theory, while

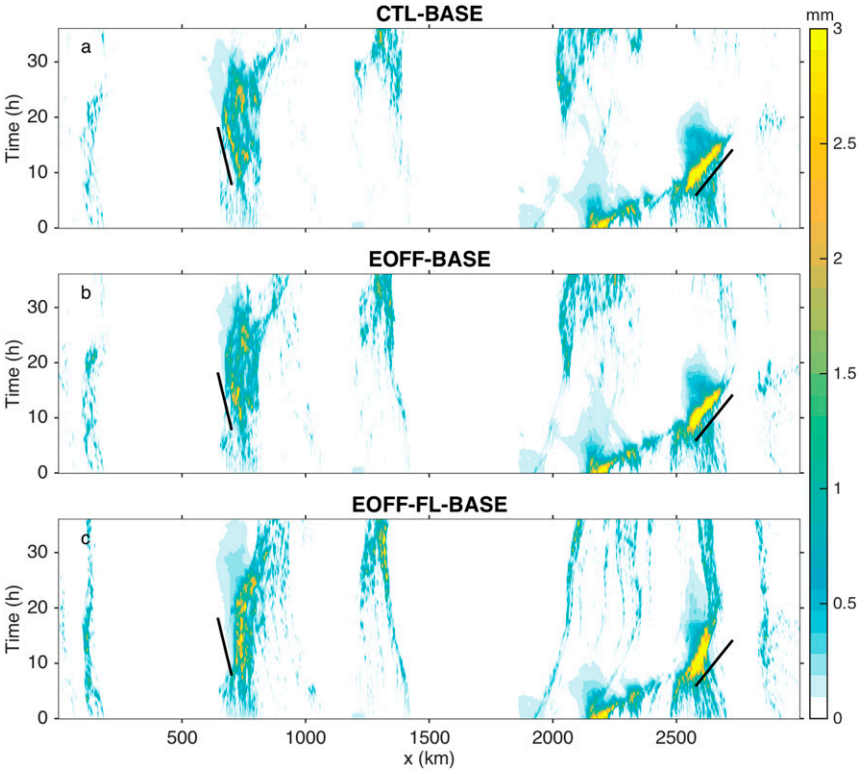

FIG. 13. Hovmöller diagrams of meridionally averaged condensed water path (mm) in (a) CTL-BASE, (b) EOFF-BASE, and (c) EOFF-FL-BASE. The black lines are in the same location in each panel in order to distinguish differences in propagation speed among the simulations.

others have not. Those studies that advocate against the use of RKW theory for tropical convective systems have found a particular reason, such as a system propagation speed that is too fast compared to the cold pool propagation speed, a propagation direction that is either parallel to the shear vector or on the upshear side of the cold pool, or a system tilt that is inconsistent with calculations of $C/\Delta u$. In this study, we have investigated the role of cold pools in influencing the intensity, mesoscale structure, propagation, and lifetime of two organized tropical oceanic convective systems. We simulated two different systems in a low–wind shear environment, one being linearly oriented and the other organized in a cluster, and then changed the cold pools by altering evaporation in the subcloud layer. If RKW theory were applicable to these tropical systems, particularly the linear system, we would expect to find changes in their intensity, mesoscale structure, and propagation speed with changes in the cold pools.

We first investigated the convective intensity response to the cold pools and found that the systems became more intense when the cold pools were weakened, in opposition to our original hypothesis. We attribute this result to the fact that the cold pool air became incorporated into the updrafts, which we verified by introducing passive tracers into the cold pools. The cold pools' negative buoyancy reduced the convective intensity on two different spatiotemporal scales: (i) on the scales of individual convective elements, the cold pool air was entrained into the updrafts and (ii) on the mesoscale, the low-level inflow air was evaporatively cooled from precipitating congestus clouds ahead of the primary convection. The detrimental influence of the cold pools on convective intensity via their negative buoyancy suggests they are not playing critical roles in initiating new convection or maintaining the existing system.

We also investigated whether our evaporation-induced changes to the cold pools influenced the mesoscale structure, propagation, or lifetimes of the convective systems. Although we saw changes in streamline tilt at low levels near the composite cold pools, neither the cluster nor the linear system exhibited differences in propagation speed, lifetime, or the broad mesoscale structure when the cold pools were altered. This confirms that RKW theory is not applicable to the behavior of these

systems, even those that otherwise appear consistent with RKW thinking. This result is highlighted by the lack of response in the linear system because its tilt and structure was in keeping with RKW thinking and the system propagation speed closely matched that of the theoretical cold pool speed. We wonder whether prior studies that have successfully applied RKW theory to tropical convective systems would also find a similar lack of response in the mesoscale structure and propagation to changes in the cold pool strengths.

Since the cold pools did not impact the convective systems' mesoscale structure or propagation, the role of gravity waves in the convective system morphology was explored. We showed the importance of the $n = 3$ wave in influencing the intensity and system evolution, in accordance with prior studies. Additionally, it appeared that this wave may be coupled to the convective systems and therefore controlled their propagation speeds. The coupling appeared to cease once the wave amplitude was artificially suppressed by removing all evaporative cooling below the freezing level. The influence of the amplitude of the $n = 3$ (and other) wave modes on their ability to couple to convection should be a topic of future research.

Our cluster and linear system results, the upshear-propagating regime (UPR) in LM15, the downshear-propagating regime (DPR) in ML15, and the shear-parallel, mei-yu front tropical system in LM17 have interesting similarities. Commonalities in structure and flow include the wave-like propagation with throughflow at all levels (linear, UPR, and mei-yu system), the tilt back over the cold pool (cluster, linear, UPR, and mei-yu system), the lack of a mesoscale downdraft (cluster, linear, and DPR), and the presence of high boundary layer humidity and relatively weak cold pools. RKW arguments do not appear to fully explain the behavior of any of these five systems, and in fact, the cold pools' inferred or demonstrated lack of importance to the propagation and structure is true for all but the UPR. However, a ducted gravity wave was also shown to be important in the UPR, and we speculate as to whether the UPR's propagation would be altered if the cold pool were eliminated. The common lack of influence of cold pools on the mesoscale features, despite the different shear strengths and orientations, suggests an important underlying cause for these similarities and their departure from midlatitude system behavior other than shear. That cause may simply be the moist boundary layer and resulting weak and shallow cold pools, which was the underlying hypothesis in LM15 and ML15.

It would be interesting to explore whether our results hold in other environments, such as tropical continental regimes. We also suggest further mechanistic studies of the role of waves in the behavior and organization of tropical convection, both from modeling and observational perspectives.

Acknowledgments. Funding support for L. D. Grant was provided by the National Science Foundation Graduate Research Fellowship Program and the Graduate Research Opportunities Worldwide program under Grant DGE-1321845. T. P. Lane was supported by the Australian Research Council's Centres of Excellence Scheme (CE170100023). S. C. van den Heever was supported by the Office of Naval Research (Grant N000141613093). High-performance computing resources were provided by the National Computational Infrastructure (NCI) facility in Canberra, Australia, and the Yellowstone supercomputer (ark:/85065/d7wd3xhc), provided by NCAR's Computational and Information Systems Laboratory and sponsored by the National Science Foundation. We thank Mitch Moncrieff for his insightful discussions and suggestions. CAPE and CIN calculations were evaluated using George Bryan's code. The comments from Stefan Tulich, two anonymous reviewers, and Matthew Parker improved the clarity and context of the manuscript and are appreciated.

REFERENCES

Adler, R. F., G. Gu, and G. J. Huffman, 2012: Estimating climatological bias errors for the Global Precipitation Climatology Project (GPCP). *J. Appl. Meteor. Climatol.*, **51**, 84–99, https://doi.org/10.1175/JAMC-D-11-052.1.

Alfaro, D. A., 2017: Low-tropospheric shear in the structure of squall lines: Impacts on latent heating under layer-lifting ascent. *J. Atmos. Sci.*, **74**, 229–248, https://doi.org/10.1175/JAS-D-16-0168.1.

Balaji, V., and T. L. Clark, 1988: Scale selection in locally forced convective fields and the initiation of deep cumulus. *J. Atmos. Sci.*, **45**, 3188–3211, https://doi.org/10.1175/1520-0469(1988)045<3188:SSILFC>2.0.CO;2.

Benjamin, T. B., 1968: Gravity currents and related phenomena. *J. Fluid Mech.*, **31**, 209–248, https://doi.org/10.1017/S0022112068000133.

Bretherton, C. S., P. N. Blossey, and M. Khairoutdinov, 2005: An energy-balance analysis of deep convective self-aggregation above uniform SST. *J. Atmos. Sci.*, **62**, 4273–4292, https://doi.org/10.1175/JAS3614.1.

Bryan, G. H., J. C. Wyngaard, and J. M. Fritsch, 2003: Resolution requirements for the simulation of deep moist convection. *Mon. Wea. Rev.*, **131**, 2394–2416, https://doi.org/10.1175/1520-0493(2003)131<2394:RRFTSO>2.0.CO;2.

Byers, H. R., and R. R. Braham Jr., 1949: *The Thunderstorm.* U.S. Government Printing Office, 287 pp.

Clark, T. L., T. Hauf, and J. P. Kuettner, 1986: Convectively forced internal gravity waves: Results from two-dimensional numerical experiments. *Quart. J. Roy. Meteor. Soc.*, **112**, 899–925, https://doi.org/10.1002/qj.49711247402.

Coniglio, M. C., S. F. Corfidi, and J. S. Kain, 2012: Views on applying RKW theory: An illustration using the 8 May 2009 derecho-producing convective system. *Mon. Wea. Rev.*, **140**, 1023–1043, https://doi.org/10.1175/MWR-D-11-00026.1.

Cotton, W. R., and Coauthors, 2003: RAMS 2001: Current status and future directions. *Meteor. Atmos. Phys.*, **82**, 5–29, https://doi.org/10.1007/s00703-001-0584-9.

Crook, N. A., and M. W. Moncrieff, 1988: The effect of large-scale convergence on the generation and maintenance of deep moist convection. *J. Atmos. Sci.*, **45**, 3606–3624, https://doi.org/10.1175/1520-0469(1988)045<3606:TEOLSC>2.0.CO;2.

DeMott, P. J., and Coauthors, 2010: Predicting global atmospheric ice nuclei distributions and their impacts on climate. *Proc. Natl. Acad. Sci. USA*, **107**, 11 217–11 222, https://doi.org/10.1073/pnas.0910818107.

Emanuel, K. A., 1994: *Atmospheric Convection.* Oxford University Press, 580 pp.

Evans, J. S., and C. A. Doswell, 2001: Examination of derecho environments using proximity soundings. *Wea. Forecasting*, **16**, 329–342, https://doi.org/10.1175/1520-0434(2001)016<0329:EODEUP>2.0.CO;2.

Fovell, R. G., 2002: Upstream influence of numerically simulated squall-line storms. *Quart. J. Roy. Meteor. Soc.*, **128**, 893–912, https://doi.org/10.1256/0035900021643737.

Grabowski, W. W., and M. W. Moncrieff, 2001: Large-scale organization of tropical convection in two-dimensional explicit numerical simulations. *Quart. J. Roy. Meteor. Soc.*, **127**, 445–468, https://doi.org/10.1002/qj.49712757211.

Grant, L. D., and S. C. van den Heever, 2016: Cold pool dissipation. *J. Geophys. Res. Atmos.*, **121**, 1138–1155, https://doi.org/10.1002/2015JD023813.

Harrington, J. Y., 1997: The effects of radiative and microphysical processes on simulated warm and transition season Arctic stratus. Ph.D. dissertation, Colorado State University, 289 pp.

Held, I. M., R. S. Hemler, and V. Ramaswamy, 1993: Radiative–convective equilibrium with explicit two-dimensional moist convection. *J. Atmos. Sci.*, **50**, 3909–3927, https://doi.org/10.1175/1520-0469(1993)050<3909:RCEWET>2.0.CO;2.

Heymsfield, G. M., L. Tian, A. J. Heymsfield, L. Li, and S. Guimond, 2010: Characteristics of deep tropical and subtropical convection from nadir-viewing high-altitude airborne Doppler radar. *J. Atmos. Sci.*, **67**, 285–308, https://doi.org/10.1175/2009JAS3132.1.

Hill, G. E., 1974: Factors controlling the size and spacing of cumulus clouds as revealed by numerical experiments. *J. Atmos. Sci.*, **31**, 646–673, https://doi.org/10.1175/1520-0469(1974)031<0646:FCTSAS>2.0.CO;2.

Houze, R. A., Jr., and C.-P. Cheng, 1977: Radar characteristics of tropical convection observed during GATE: Mean properties and trends over the summer season. *Mon. Wea. Rev.*, **105**, 964–980, https://doi.org/10.1175/1520-0493(1977)105<0964:RCOTCO>2.0.CO;2.

Jeevanjee, N., and D. M. Romps, 2013: Convective self-aggregation, cold pools, and domain size. *Geophys. Res. Lett.*, **40**, 994–998, https://doi.org/10.1002/grl.50204.

Johnson, R. H., S. L. Aves, P. E. Ciesielski, and T. D. Keenan, 2005: Organization of oceanic convection during the onset of the 1998 East Asian summer monsoon. *Mon. Wea. Rev.*, **133**, 131–148, https://doi.org/10.1175/MWR-2843.1.

Keenan, T. D., and R. E. Carbone, 1992: A preliminary morphology of precipitation systems in tropical northern Australia. *Quart. J. Roy. Meteor. Soc.*, **118**, 283–326, https://doi.org/10.1002/qj.49711850406.

Klemp, J. B., and R. B. Wilhelmson, 1978: The simulation of three-dimensional convective storm dynamics. *J. Atmos. Sci.*, **35**, 1070–1096, https://doi.org/10.1175/1520-0469(1978)035<1070:TSOTDC>2.0.CO;2.

Lac, C., J.-P. Lafore, and J.-L. Redelsperger, 2002: Role of gravity waves in triggering deep convection during TOGA COARE. *J. Atmos. Sci.*, **59**, 1293–1316, https://doi.org/10.1175/1520-0469(2002)059<1293:ROGWIT>2.0.CO;2.

Lane, T. P., and M. J. Reeder, 2001: Convectively generated gravity waves and their effect on the cloud environment. *J. Atmos. Sci.*, **58**, 2427–2440, https://doi.org/10.1175/1520-0469(2001)058<2427:CGGWAT>2.0.CO;2.

——, and M. W. Moncrieff, 2008: Stratospheric gravity waves generated by multiscale tropical convection. *J. Atmos. Sci.*, **65**, 2598–2614, https://doi.org/10.1175/2007JAS2601.1.

——, and ——, 2010: Characterization of momentum transport associated with organized moist convection and gravity waves. *J. Atmos. Sci.*, **67**, 3208–3225, https://doi.org/10.1175/2010JAS3418.1.

——, and F. Zhang, 2011: Coupling between gravity waves and tropical convection at mesoscales. *J. Atmos. Sci.*, **68**, 2582–2598, https://doi.org/10.1175/2011JAS3577.1.

——, and M. W. Moncrieff, 2015: Long-lived mesoscale systems in a low–convective inhibition environment. Part I: Upshear propagation. *J. Atmos. Sci.*, **72**, 4297–4318, https://doi.org/10.1175/JAS-D-15-0073.1.

LeMone, M. A., and E. J. Zipser, 1980: Cumulonimbus vertical velocity events in GATE. Part I: Diameter, intensity and mass flux. *J. Atmos. Sci.*, **37**, 2444–2457, https://doi.org/10.1175/1520-0469(1980)037<2444:CVVEIG>2.0.CO;2.

——, ——, and S. B. Trier, 1998: The role of environmental shear and thermodynamic conditions in determining the structure and evolution of mesoscale convective systems during TOGA COARE. *J. Atmos. Sci.*, **55**, 3493–3518, https://doi.org/10.1175/1520-0469(1998)055<3493:TROESA>2.0.CO;2.

Liu, C., and M. W. Moncrieff, 2004: Effects of convectively generated gravity waves and rotation on the organization of convection. *J. Atmos. Sci.*, **61**, 2218–2227, https://doi.org/10.1175/1520-0469(2004)061<2218:EOCGGW>2.0.CO;2.

——, and E. Zipser, 2013: Regional variation of morphology of organized convection in the tropics and subtropics. *J. Geophys. Res. Atmos.*, **118**, 453–466, https://doi.org/10.1029/2012JD018409.

——, and M. W. Moncrieff, 2017: Shear-parallel mesoscale convective systems in a moist low-inhibition mei-yu front environment. *J. Atmos. Sci.*, **74**, 4213–4228, https://doi.org/10.1175/JAS-D-17-0121.1.

Louis, J.-F., 1979: A parametric model of vertical eddy fluxes in the atmosphere. *Bound.-Layer Meteor.*, **17**, 187–202, https://doi.org/10.1007/BF00117978.

Lucas, C., E. J. Zipser, and M. A. Lemone, 1994: Vertical velocity in oceanic convection off tropical Australia. *J. Atmos. Sci.*, **51**, 3183–3193, https://doi.org/10.1175/1520-0469(1994)051<3183:VVIOCO>2.0.CO;2.

Manabe, S., and R. F. Strickler, 1964: Thermal equilibrium of the atmosphere with a convective adjustment. *J. Atmos. Sci.*, **21**, 361–385, https://doi.org/10.1175/1520-0469(1964)021<0361:TEOTAW>2.0.CO;2.

Mapes, B. E., 1993: Gregarious tropical convection. *J. Atmos. Sci.*, **50**, 2026–2037, https://doi.org/10.1175/1520-0469(1993)050<2026:GTC>2.0.CO;2.

McGee, C. J., and S. C. van den Heever, 2014: Latent heating and mixing due to entrainment in tropical deep convection. *J. Atmos. Sci.*, **71**, 816–832, https://doi.org/10.1175/JAS-D-13-0140.1.

Meyers, M. P., R. L. Walko, J. Y. Harrington, and W. R. Cotton, 1997: New RAMS cloud microphysics parameterization.

Part II: The two-moment scheme. *Atmos. Res.*, **45**, 3–39, https://doi.org/10.1016/S0169-8095(97)00018-5.

Moncrieff, M. W., and M. J. Miller, 1976: The dynamics and simulation of tropical cumulonimbus and squall lines. *Quart. J. Roy. Meteor. Soc.*, **102**, 373–394, https://doi.org/10.1002/qj.49710243208.

——, and T. P. Lane, 2015: Long-lived mesoscale systems in a low–convective inhibition environment. Part II: Downshear propagation. *J. Atmos. Sci.*, **72**, 4319–4336, https://doi.org/10.1175/JAS-D-15-0074.1.

Muller, C., and S. Bony, 2015: What favors convective aggregation and why? *Geophys. Res. Lett.*, **42**, 5626–5634, https://doi.org/10.1002/2015GL064260.

Nesbitt, S. W., E. J. Zipser, and D. J. Cecil, 2000: A census of precipitation features in the tropics using TRMM: Radar, ice scattering, and lightning observations. *J. Climate*, **13**, 4087–4106, https://doi.org/10.1175/1520-0442(2000)013<4087:ACOPFI>2.0.CO;2.

——, R. Cifelli, and S. A. Rutledge, 2006: Storm morphology and rainfall characteristics of TRMM precipitation features. *Mon. Wea. Rev.*, **134**, 2702–2721, https://doi.org/10.1175/MWR3200.1.

Nicholls, M. E., R. H. Johnson, and W. R. Cotton, 1988: The sensitivity of two-dimensional simulations of tropical squall lines to environmental profiles. *J. Atmos. Sci.*, **45**, 3625–3649, https://doi.org/10.1175/1520-0469(1988)045<3625:TSOTDS>2.0.CO;2.

Pandya, R. E., and D. R. Durran, 1996: The influence of convectively generated thermal forcing on the mesoscale circulation around squall lines. *J. Atmos. Sci.*, **53**, 2924–2951, https://doi.org/10.1175/1520-0469(1996)053<2924:TIOCGT>2.0.CO;2.

Parker, M. D., and R. H. Johnson, 2004: Simulated convective lines with leading precipitation. Part I: Governing dynamics. *J. Atmos. Sci.*, **61**, 1637–1655, https://doi.org/10.1175/1520-0469(2004)061<1637:SCLWLP>2.0.CO;2.

Posselt, D. J., S. C. van den Heever, and G. L. Stephens, 2008: Trimodal cloudiness and tropical stable layers in simulations of radiative convective equilibrium. *Geophys. Res. Lett.*, **35**, L08802, https://doi.org/10.1029/2007GL033029.

——, ——, ——, and M. R. Igel, 2012: Changes in the interaction between tropical convection, radiation, and the large-scale circulation in a warming environment. *J. Climate*, **25**, 557–571, https://doi.org/10.1175/2011JCLI4167.1.

Raymond, D. J., 1994: Convective processes and tropical atmospheric circulations. *Quart. J. Roy. Meteor. Soc.*, **120**, 1431–1455, https://doi.org/10.1002/qj.49712052002.

——, 1995: Regulation of moist convection over the west Pacific warm pool. *J. Atmos. Sci.*, **52**, 3945–3959, https://doi.org/10.1175/1520-0469(1995)052<3945:ROMCOT>2.0.CO;2.

Riehl, H., and J. S. Malkus, 1958: On the heat balance in the equatorial trough zone. *Geophysica*, **6**, 503–538.

Robe, F. R., and K. A. Emanuel, 2001: The effect of vertical wind shear on radiative–convective equilibrium states. *J. Atmos. Sci.*, **58**, 1427–1445, https://doi.org/10.1175/1520-0469(2001)058<1427:TEOVWS>2.0.CO;2.

Rotunno, R., J. B. Klemp, and M. L. Weisman, 1988: A theory for strong, long-lived squall lines. *J. Atmos. Sci.*, **45**, 463–485, https://doi.org/10.1175/1520-0469(1988)045<0463:ATFSLL>2.0.CO;2.

Saleeby, S. M., and W. R. Cotton, 2004: A large-droplet mode and prognostic number concentration of cloud droplets in the Colorado State University Regional Atmospheric Modeling System (RAMS). Part I: Module descriptions and supercell test simulations. *J. Appl. Meteor.*, **43**, 182–195, https://doi.org/10.1175/1520-0450(2004)043<0182:ALMAPN>2.0.CO;2.

——, and ——, 2008: A binned approach to cloud-droplet riming implemented in a bulk microphysics model. *J. Appl. Meteor. Climatol.*, **47**, 694–703, https://doi.org/10.1175/2007JAMC1664.1.

——, and S. C. van den Heever, 2013: Developments in the CSU-RAMS aerosol model: Emissions, nucleation, regeneration, deposition, and radiation. *J. Appl. Meteor. Climatol.*, **52**, 2601–2622, https://doi.org/10.1175/JAMC-D-12-0312.1.

Schumacher, C., S. N. Stevenson, and C. R. Williams, 2015: Vertical motions of the tropical convective cloud spectrum over Darwin, Australia. *Quart. J. Roy. Meteor. Soc.*, **141**, 2277–2288, https://doi.org/10.1002/qj.2520.

Schumacher, R. S., 2015: Sensitivity of precipitation accumulation in elevated convective systems to small changes in low-level moisture. *J. Atmos. Sci.*, **72**, 2507–2524, https://doi.org/10.1175/JAS-D-14-0389.1.

Shige, S., and T. Satomura, 2001: Westward generation of eastward-moving tropical convective bands in TOGA COARE. *J. Atmos. Sci.*, **58**, 3724–3740, https://doi.org/10.1175/1520-0469(2001)058<3724:WGOEMT>2.0.CO;2.

Smagorinsky, J., 1963: General circulation experiments with the primitive equations. I. The basic experiment. *Mon. Wea. Rev.*, **91**, 99–164, https://doi.org/10.1175/1520-0493(1963)091<0099:GCEWTP>2.3.CO;2.

Stensrud, D. J., M. C. Coniglio, R. P. Davies-Jones, and J. S. Evans, 2005: Comments on "'A theory for strong long-lived squall lines' revisited." *J. Atmos. Sci.*, **62**, 2989–2996, https://doi.org/10.1175/JAS3514.1.

Stephens, G. L., 1990: On the relationship between water vapor over the oceans and sea surface temperature. *J. Climate*, **3**, 634–645, https://doi.org/10.1175/1520-0442(1990)003<0634:OTRBWV>2.0.CO;2.

——, N. B. Wood, and L. A. Pakula, 2004: On the radiative effects of dust on tropical convection. *Geophys. Res. Lett.*, **31**, L23112, https://doi.org/10.1029/2004GL021342.

——, S. van den Heever, and L. Pakula, 2008: Radiative–convective feedbacks in idealized states of radiative–convective equilibrium. *J. Atmos. Sci.*, **65**, 3899–3916, https://doi.org/10.1175/2008JAS2524.1.

Storer, R. L., and S. C. van den Heever, 2013: Microphysical processes evident in aerosol forcing of tropical deep convective clouds. *J. Atmos. Sci.*, **70**, 430–446, https://doi.org/10.1175/JAS-D-12-076.1.

Tan, J., C. Jakob, and T. P. Lane, 2013: On the identification of the large-scale properties of tropical convection using cloud regimes. *J. Climate*, **26**, 6618–6632, https://doi.org/10.1175/JCLI-D-12-00624.1.

Tompkins, A. M., 2001: Organization of tropical convection in low vertical wind shears: The role of cold pools. *J. Atmos. Sci.*, **58**, 1650–1672, https://doi.org/10.1175/1520-0469(2001)058<1650:OOTCIL>2.0.CO;2.

——, and G. C. Craig, 1998: Radiative–convective equilibrium in a three-dimensional cloud-ensemble model. *Quart. J. Roy. Meteor. Soc.*, **124**, 2073–2097, https://doi.org/10.1002/qj.49712455013.

Torri, G., and Z. Kuang, 2016: A Lagrangian study of precipitation-driven downdrafts. *J. Atmos. Sci.*, **73**, 839–854, https://doi.org/10.1175/JAS-D-15-0222.1.

——, ——, and Y. Tian, 2015: Mechanisms for convection triggering by cold pools. *Geophys. Res. Lett.*, **42**, 1943–1950, https://doi.org/10.1002/2015GL063227.

Trier, S. B., J. H. Marsham, C. A. Davis, and D. A. Ahijevych, 2011: Numerical simulations of the postsunrise reorganization of a nocturnal mesoscale convective system during 13 June IHOP_2002. *J. Atmos. Sci.*, **68**, 2988–3011, https://doi.org/10.1175/JAS-D-11-0112.1.

Tulich, S. N., and B. E. Mapes, 2008: Multiscale convective wave disturbances in the tropics: Insights from a two-dimensional

cloud-resolving model. *J. Atmos. Sci.*, **65**, 140–155, https://doi.org/10.1175/2007JAS2353.1.

——, and G. N. Kiladis, 2012: Squall lines and convectively coupled gravity waves in the tropics: Why do most cloud systems propagate westward? *J. Atmos. Sci.*, **69**, 2995–3012, https://doi.org/10.1175/JAS-D-11-0297.1.

Varble, A., and Coauthors, 2014: Evaluation of cloud-resolving and limited area model intercomparison simulations using TWP-ICE observations: 1. Deep convective updraft properties. *J. Geophys. Res. Atmos.*, **119**, 13 891–13 918, https://doi.org/10.1002/2013JD021371.

Walko, R. L., W. R. Cotton, G. Feingold, and B. Stevens, 2000: Efficient computation of vapor and heat diffusion between hydrometeors in a numerical model. *Atmos. Res.*, **53**, 171–183, https://doi.org/10.1016/S0169-8095(99)00044-7.

Webster, P. J., and Coauthors, 2002: The JASMINE pilot study. *Bull. Amer. Meteor. Soc.*, **83**, 1603–1630, https://doi.org/10.1175/BAMS-83-11-1603.

Weisman, M. L., and R. Rotunno, 2004: ''A theory for strong long-lived squall lines'' revisited. *J. Atmos. Sci.*, **61**, 361–382, https://doi.org/10.1175/1520-0469(2004)061<0361:ATFSLS>2.0.CO;2.

Zipser, E. J., 1977: Mesoscale and convective-scale downdrafts as distinct components of squall-line structure. *Mon. Wea. Rev.*, **105**, 1568–1589, https://doi.org/10.1175/1520-0493(1977)105<1568:MACDAD>2.0.CO;2.